# Fermi velocities in silver: Surface Landau-level resonances

John W. Mitchell and R. G. Goodrich
*Department of Physics and Astronomy, Louisiana State University, Baton Rouge, Louisiana 70803-4001*
(Received 29 April 1985; revised manuscript received 11 July 1985)

Local values of the Fermi velocity of Ag are determined along the central zones of the (100) and (110) sample planes and at the neck in the (111) plane. Resonance spectra of magnetic-field-induced quantum-surface states, known as surface Landau-level resonances (SLLR), are used along with geometric factors calculated from analytical expressions for the Fermi surface to determine the location and Fermi velocity of the resonant electrons by an iterative process. These velocities are compared to those previously derived from inversions of cyclotron mass data.

## INTRODUCTION

The most accurately known Fermi surfaces (FS's) of any metals are those of Cu, Ag, and Au.[1] The **k**-space coordinates of any point on the Fermi surface (FS) of these metals can be obtained from analytical expressions, in the form of symmetrized Fourier expansions (SFE's), to an accuracy of 0.2%.[1,2] In addition, inversions of cyclotron masses have been performed to yield similar analytical expressions for the Fermi velocity $v_F$ at all points on these surfaces.[2,3]

The SFE expression of Ref. 1 predicts points on the FS of all three metals to within the accuracy of all published experimental data as does that of Ref. 2 for Cu and Ag. However, the expressions for $v_F$ have not been as successful. Local values of $v_F$ can only be found from the cyclotron mass data by a complicated deconvolution process requiring a detailed knowledge of the FS and so must be regarded as somewhat approximate. The only current experimental techniques for obtaining localized values of $v_F$ directly are the measurements of surface Landau-level resonances (SLLR's) (Ref. 4) and the time-of-flight effect (TFE) (Refs. 5 and 6). On the basis of SLLR measurements, Doezema and Koch (DK) (Ref. 7) have found deviations from Halse's[2] expression for $v_F$ of up to 6% along (100) in Cu. Their results show better agreement with the Korringa-Kohn-Rostoker (KKR) phase-shift analysis of Lee,[8] although substantial deviations, on the order of 3%, are found at various points on the FS. Considerably better agreement is found with the more recent measurements reported by Lengeler *et al.*,[3] which were not available at the time of the work reported by DK. Two SLLR experiments have been reported for Ag.[9,10] In both of these experiments the spectra obtained were of poor quality and the agreement with Halse's values of $v_F$ at selected points on the FS was not good. Although they were not available when these SLLR experiments were conducted, the Lengeler values of $v_F$ show even less agreement, with a difference, from the results of Deimel and Doezema,[10] of 15% at ⟨100⟩ in the (110) plane. There have been no SLLR measurements reported for Au.

In this report we give the results of our measurements of SLLR signals in Ag, motivated in part by these large discrepancies, and compare the derived $v_F$ distribution for the (100), (110), and (111) cross sections of the FS to the existing analytical models. This is the first of two papers aimed at determining both the Fermi velocities and anisotropic electron-phonon relaxation times on the FS of Ag.

A surface-energy-level spectrum is observed in SLLR measurements associated with electrons bound to the surface of the metal by an applied magnetic field. The magnetic field is applied parallel to a highly polished metal surface and conduction electrons near the surface are confined in a triangular potential well between the surface potential and a potential, due to the Lorentz force, which increases linearly with depth into the metal. Classically, this corresponds to electrons traveling nearly parallel to the metal surface being specularly reflected at the surface and returning to the surface under the turning influence of the applied magnetic field, in what have come to be known as skipping orbits. The allowed electron states in the potential well correspond to a series of quantum energy levels and it is possible to observe transitions between these levels induced by microwave radiation incident on the sample at frequency $\omega$. The separation between levels depends on the strength of the applied magnetic field and resonant absorption of the radiation occurs when the resonance condition

$$H_{mn}=\frac{\hbar}{e}\left[\frac{\omega}{a_n-a_m}\right]^{3/2}\left[\frac{2K}{v_F^3}\right]_{\perp}^{1/2}$$

is met.[4,7] Here $H_{mn}$ is the magnitude of the applied magnetic field for transitions between the $m$ and $n$ levels, and $K$ is the **k**-space radius of curvature of the resonant-electron orbit. The $a_n$ are the zeros of the Airy function and the symbol $\perp$ indicates that the components of both $K$ and $v_F$ perpendicular to the magnetic field direction are to be used. Following the notation of DK, we define the expected field value of the (1-2) transition to be $H_p$ and the scaling factor $(a_2-a_1)^{-3/2}$ to be $h_p$. Typical resonant fields observed in this experiment are in the range of 1—100 Oe at a frequency of 35 GHz.

In a SLLR experiment, the first derivative of the real part of the surface impedance of the metal with respect to magnetic field, $dR/dH$, is measured as a function of applied field. Since the power absorption at resonance is proportional to $\mathbf{v}\cdot\mathbf{E}$ and since the microwave electric field

 

E is parallel to the metal surface, the resonant electrons must be on a portion of the FS where $v_F$ is nearly parallel to the sample surface. Electrons in skipping orbits meet this condition since the radius of curvature of the skipping orbit ($\sim 1$ cm) is large compared to the microwave skin depth of $10^{-5}$ cm and those electrons which remain within the skin-depth region longest make the largest contribution to the signal. In addition, the skipping orbits must pass through a point where $k_z$, the component of electron momentum normal to the sample surfaces, is zero. These conditions imply that the contributing electrons travel nearly parallel to the sample surface and lie on a narrow ($\sim \pm 0.5°$) band around the $k_z=0$ region on the FS. At any point along this band the values of $K_\perp$ and $v_{F\perp}$ depend on the component of the Fermi radius, $k_H$, in the direction of $H$. Peaks in $dR/dH$ are observed when $K_\perp$ and $v_{F_\perp}$ are such that the resonance condition $H_{mn}(k_H)$ is extremal. In addition, there are three factors having secondary effects on the observed values of the resonant fields: the resonant-electron lifetime, the microwave skin depth, and the manner in which $H_{mn}(k_H)$ varies around the extremal location. Taking these effects into account, the extremal values of the resonance parameter $R=(K/v_F^3)_\perp^{1/2}$ may be derived from measurements of the field positions of the resonance peaks and may be used, along with an assignment of the locations on the FS to which the extrema correspond, to determine $v_F$ at these locations. In making this determination, we follow the method of DK for Cu and assume that the FS geometry of Ag is known precisely from analytical expressions.[1,2] At points of high symmetry in the orientation of the magnetic field with respect to the FS, values of $v_F$ are determined uniquely from the field value at resonance. However, at general points on the FS, including most intersections of the FS with symmetry planes, both $K$ and $v_F$ must be known to locate the extremal positions. Since we only consider the value of $K$ to be known at any given point on the FS, an iterative procedure, based on the experimental values of $H_p$ and beginning from a model for the $v_F$ distribution, is used to determine the resonant points on the FS. The small corrections to the field positions due to lifetimes, skin depth, and the variation of $H_p(k_H)$ are taken into account prior to the iteration procedure.

## EXPERIMENTAL

The samples used in this experiment were obtained from a large single crystal grown by a modified Bridgman technique. The starting material for these crystals was purchased from Cominco, Inc. and had a quoted purity of 99.9999%. A single-crystal boule was grown in a tapered graphite crucible and oriented samples for the SLLR measurements were cut by spark erosion from the crystal. Before cutting, the bulk crystal was oxygen annealed and had a measured residual-resistance ratio after annealing in excess of 25 000. After cutting, the individual samples were again annealed by heating to 900 °C in a vacuum, adding an $O_2$ flow at a pressure of $4\times 10^4$ Torr for 18 h, then evacuating the furnace and cooling at 15 °C/h. Since the preparation of the surfaces of these samples is of critical importance in obtaining results, the method by which this was done is described here in some detail.

A chemical polishing machine was used to achieve the flat, strain-free surfaces desired. The machine consists of a horizontally rotating 12-in.-diam. ground-glass disk covered with a cloth and a rotating sample holder which maintains the sample surface parallel to the disk surface. Acid is applied to the cloth and the sample is rotated in the same direction as the glass plate. The acid used consisted of 61.7 g $CrO_3$, 11.8 ml HCl (38% reagent grade), and 933 ml $H_2O$. The silver removal rate can be varied by varying the temperature of the solution and is on the order of 0.25 mm/h at 5 °C. The type of cloth used is important to the final result and we have been most successful with an interlock-weave Quiana nylon. Cotton of the same weave works well, but deteriorates in the acid. The sample is placed in light contact with the cloth and its rotation rate adjusted to equalize the relative velocity of the cloth across the sample surface. The best results were obtained with the cloth moving at $1.3\times 10^2$ mm/sec relative to the sample. When the sample is lifted from the cloth it is immediately washed with $H_2O$ to stop the acid reaction. After polishing, a thin film remains on the surface and must be removed with dilute phosphoric acid. Following this, the sample is again washed in $H_2O$ for an extended period to ensure that all acid reactions are completely stopped. Next, the sample is removed from the holder and undergoes two additional washes; first in toluene and then in ethyl alcohol. The sample is mounted on the microwave cavity and the sample holder is evacuated as quickly as possible to reduce oxidation of the surface.

The samples prepared in this manner form the end wall of a 35-GHz microwave cavity operating in the $TE_{111}$ mode with a loaded $Q$ of about 10 000. A standard, Gunn-oscillator-driven microwave spectrometer was used with lock-in detection to record $dR/dH$ as a function of applied magnetic field. The field was produced by a rotatable Helmholtz pair surrounded by three additional mutually perpendicular coil pairs used to reduce the effect of the earth's field to less than $10^{-2}$ Oe at the sample location. The applied field was calibrated at the sample position at low fields (1.9—4.1 Oe) from the EPR signal of a free radical[11] (5.4—11.6 MHz) and around 100 OE from proton NMR.

## PEAK DISTRIBUTIONS AND LINE-SHAPE CONSIDERATIONS

In order to perform the iterative calculation of $v_F$ described above, an assignment of the location of the resonant electrons on the FS is required as a starting model. To provide such a model as well as to give an immediate comparison to our experimental spectra, we have calculated the distribution of expected (1-2) peak-field values $H_p$ as a function of field orientation using the analytical expressions for $v_F$ and $k_F$ as our basis. The analytical expressions give a value of $v_F$ which is reduced from the band velocity by a factor of $[1+\lambda(\mathbf{k})]^{-1}$, where $\lambda(\mathbf{k})$ is the electron-phonon enhancement factor. Since the SLLR measurements are taken at a temperature of $\sim 1.5$ K,where electron-phonon enhancement is fully ef-

fective, the velocities obtained are reduced by the same factor. For consistency of presentation, we have chosen the seven-term **k** fit of Coleridge and Templeton (CT) (Ref. 1) as the basis for our calculations although we have performed the complete range of calculations using Halse's Ag7 **k** fit with essentially indistinguishable results. This is not true of the $v_F$ fits, and in view of their differences, we present projected peak distributions based on both the Halse and Lengeler expressions.

In order to generate a resonant peak distribution we must, for each magnetic field orientation, calculate the resonance parameter $R$ for closely spaced points around the zone of interest. This is done over a sufficiently wide angular range to cover both the crystal symmetry and the full range of possible angles between the magnetic field direction and the direction of the normal to the zone perimeter. In practice, this means that the calculation must be performed over a 180° range. Both $v_F$ and $K$ are parallel to the normal and so, if the normal direction is determined at each FS location, $(K/v_F^3)_\perp^{1/2}$ is simply $(K/v_F^3)^{1/2}/(\cos\alpha)$ where $\alpha$ is the angle between the field direction and the normal.

The resonances expected at a particular field orientation are the $H_{mn}$ found from the extremal values of $R$. The identification of the FS location of these resonances using the SFE expressions for $v_F$ provides a starting point for determining the origin of the experimental signals.

Although the principal contribution to the experimental lines at a particular field orientation are those electrons for which the resonance parameter is extremal, there is some contribution to the signal from electrons located over a relatively large ($\sim\pm 6°$) range around the extremal position. The effect of these nonextremal electrons, known as $k_H$ broadening, is to widen the experimental lines and to shift the peak away from its extremal value. For minima in $R$ the nonextremal electrons undergo transitions at higher field and their inclusion in the signal tends to shift the peak up in field. The opposite is true for lines arising from electrons where $R$ is maximal. The degree to which the experimental peak is shifted depends on the values of two additional line-shape-fitting parameters, $\Gamma^* = 1/\omega\tau$ and

$$\beta = \frac{1}{(2\omega)^{1/2}} \left[\frac{v_F}{K}\right]_\perp^{1/2} \frac{1}{\delta},$$

where $\delta$ is the anomalous-skin-effect (ASE) skin depth and $\tau$ the electron relaxation time. These must be determined from line-shape considerations applied to the experimental spectra, a typical example of which is given in Fig. 1. Characteristic line shapes for a variety of $\beta$ and $\Gamma^*$ can be generated using expressions derived by Nee, Koch, and Prange (NKP).[4] For experimental spectra, $\Gamma^*$ is calculated from the half-width of the (1-2) peak[12,13] and $\beta$ is determined by comparison to the NKP spectra for this $\Gamma^*$. In principle, this determination must be made for each set of experimental data, although in practice we only determine $\Gamma^*$ directly. Then, for each sample, we determine $\beta$ at a well-known FS location such as the (100) point in the (100) and (110) planes and scale this value by the appropriate $v_F$ and $K$ to find $\beta$ at other locations. We

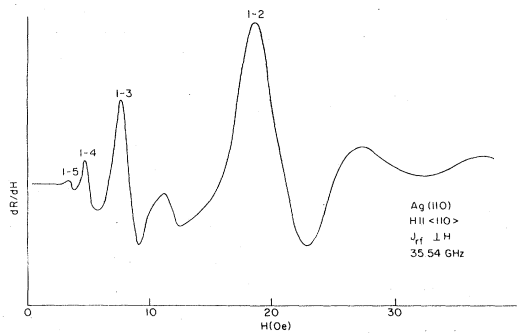


FIG. 1. Experimental $dR/dH$ resonance spectrum observed at 1.9 K in the (110) simple plane of Ag. The principal series corresponds to point $a$ of Fig. 3.

estimate this scaling procedure to be certain to better than 0.5%. The basic assignment of $\beta$ is, however, somewhat less certain and its determination is one of the limiting factors in the accuracy to which $v_F$ can be calculated.

These line-shape factors, as well as the calculation of $k_H$ broadening effects have been treated extensively elsewhere[4,7,13] and we have followed the technique of DK,[7] including the use of a library of NKP characteristic spectra, in dealing with them. Their analysis was performed for idealized cylindrical and spherical FS geometries and, since the Ag FS is considerably more spherical than that of Cu, is directly applicable to our work.

The more spherical FS of Ag may also, in part, explain the broader resonance lines seen in this experiment as well as in the previously published studies of Ag.[9,10] Our linewidths, while substantially narrower and better defined than those seen in previous experiments, are still quite broad compared to those seen by DK in Cu. This may result from the fact that the local radius of curvature in the effective plane at the resonant-electron location is often smaller in copper. This means that even though the

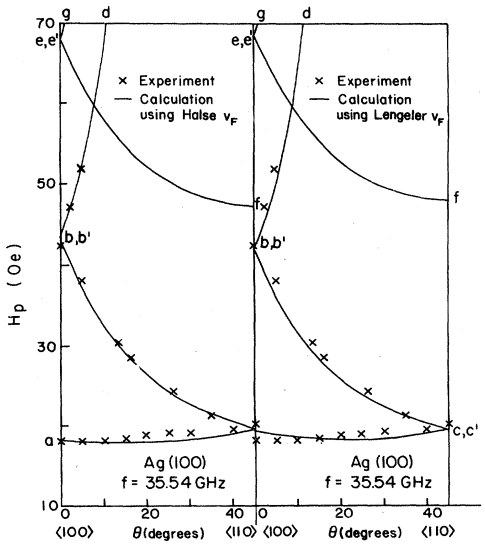


FIG. 2. Predicted and observed distributions of (1-2) resonance peaks in the (100) plane at Ag as a function of $\theta$, the angle between the magnetic field direction and the ⟨010⟩ axis.

linewidth may saturate at the same angle measured from an origin at the center of curvature in both metals, in Cu this represents a smaller angle measured with respect to the center of the FS, and so a relatively smaller region of FS is represented in the signal. This would tend to make the averaging effect of $k_H$ broadening greater in Ag. Although, if anything, this means that Ag conforms even more closely than Cu to the model calculations made by DK. We consider these effects to be well understood and that, despite the broadening effects discussed above, the final Fermi velocities may be taken as being quite well localized at the extremal electron position.

## EXPERIMENTAL RESULTS

The values of $H_p$ measured for the (100) and (110) sample planes are shown in Fig. 2 along with the predicted $H_p$ values for the SFE $v_F$ fits. The $h_p$ values used in these calculations were derived from line-shape analysis of the corresponding experimental spectra in order to make possible a direct comparison of the experimental and calculated peak distributions. The resonant-electron locations corresponding to the $H_p$ plots in Figs. 2 and 3 are given in Fig. 4, showing the cumulative region of FS to which our measurements apply. The details of the manner in which the predicted $H_p$ values were calculated as well a discussion of the assignment of resonant electron locations may be found in Ref. 14.

Analysis of the (111) sample-plane data proved somewhat more difficult than that in the (100) and (110) planes. The relative amplitude of the neck signal, at 26.3 Oe, was found to be less than some of the other signals detected and was identified by two distinctive characteristics. First, it was constant in field over a better than 180° range of external field orientation, and second, its amplitude decreased as the angle between $J_{rf}$ and $H$ was decreased from 90°. This is expected for a circular neck geometry and an isotropic $v_F$ distribution since, under these conditions, the effective electron location should always be such that $v_F$ is perpendicular to $H$ and, as a result, the signal amplitude is expected to decrease as the cosine of the angle between $v_F$ and $J_{rf}$. Our observation of both of these effects is a strong argument for an isotropic, circular neck.

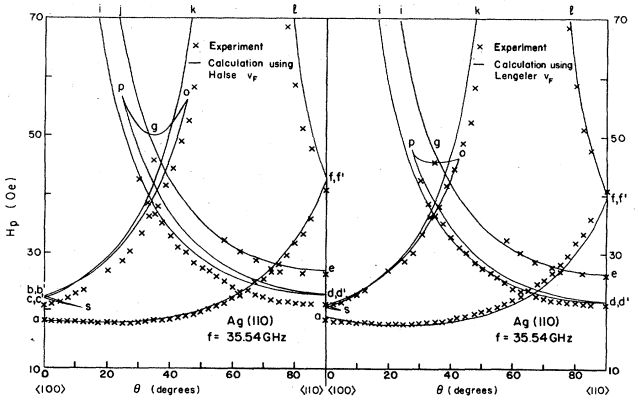


FIG. 3. Predicted and observed distributions of (1-2) resonance peaks in the (110) plane of Ag as a function of $\theta$, the angle between the magnetic field direction and the ⟨110⟩ axis. The observed peak marked near point $g$ is scaled from the neck value measured in the (111) plane.

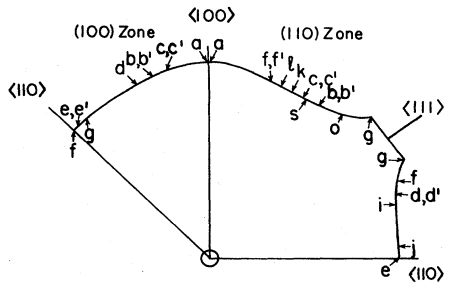


FIG. 4. Fermi-surface locations of electrons corresponding to resonance series shown in Fig. 2 for the (100) plane and in Fig. 3 for the (110) plane. These ranges represent a mapping of the derived Fermi-surface locations onto one cycle of crystal symmetry.

Our method of computing FS parameters did not rely on the reduction of the SFE expression for the FS to a cubic equation as did that of DK, and so it is possible to identify the anisotropic resonances observed in this plane. Since this analysis was not possible with the method used by DK, we will briefly discuss our results. The $k_z=0$ region on the FS must first be identified. The FS is not symmetric about the (111) central plane, except at the ⟨110⟩ points, and these are the only points on the intersection of the FS and the central plane for which $k_z=0$. Away from a particular ⟨110⟩ point, the locations of the $k_z=0$ points fall near the portion of the intersection of the FS and a (110) central plane which contains that ⟨110⟩ point. Along this region the resonance parameter $R$ is nearly constant and in this sense the region may be regarded as cylinder-like. Symmetry considerations lead to the conclusion that for $\mathbf{H}\|[112]$ the extremal location should be at ⟨110⟩. As $\mathbf{H}$ is rotated away from [112] the extremal location moves slowly along the $k_z=0$ region. Because of the slow variation in $R$, significant contributions to the signal are expected from electrons over a relatively large range around the extremal point.

As reported in Ref. 13, we have used the temperature dependence of the line shape of signals due to electrons on this cylinder-like region in analyzing the (111) neck resonance. An unfolding process was used to remove the effect of a partially overlapping peak, allowing an accurate determination of the peak position and line shape of the neck signal.

## FERMI VELOCITIES

In calculating $v_F$ from our experimental data, we have taken an approach somewhat different from but equivalent to the iterative scheme used by DK. We first identify those points for which an *a priori* assignment of location can be made. The experimental peak values measured at these points together with our assumed geometry give an immediate measure of the value of $v_F$.

For other points we resort to an iterative procedure.

Since we have already, as discussed above, generated distributions of peak-field values and corresponding electron locations from the SFE velocity distributions, we can use these as starting models. For this purpose we have used the Lengeler velocity distribution, although the Halse distribution would have done equally well. Using the model distribution, we assign to the experimental peaks at each field orientation the FS location of the corresponding calculated peaks. We use the geometric factors calculated at these locations along with the experimental $H_p$ values to produce a point-by-point velocity distribution over the measured region and map this distribution onto a single cycle of crystal symmetry. We then fit the distribution to a polynomial of the form

$$v_F = C_0 + C_1\phi + C_2\phi^2 + \cdots$$

using a nonlinear least-squares procedure. This gives an analytical expression for $v_F$ as a function of $\phi$ which, in turn, is used to generate new extremal values of the resonance parameter and, finally, new resonant-electron locations. The procedure is repeated until the locations converge to within the desired precision ($\sim 0.1°$). Typically this has been reached after three iterations. A check on the validity of our fit is that the change in location from the assumed model is small, where the correspondence between experimental and predicted peaks is good. The *a priori* locations remained fixed, although no special care was taken to ensure this. This pointwise assignment of resonant electron location allows, as a final step, the calculation of $v_F$ at these locations using their associated geometric factors and the corresponding experimental $H_p$ values. Details of these calculations are found in Ref. 14.

A fifth-order polynomial was used to fit the (110)-plane $v_F$ distribution, while the relatively less complex (100)-plane distribution was fit with a fourth-order polynomial. The (110)-plane fit applies over the range of $\phi = 0°$ to the neck at $\phi = 47.72°$ with a second polynomial applicable over the range from the neck at $\phi = 61.76°$ to $\phi = 71°$, while the (100) fit applies over the range $\phi = 0°$ to $\phi = 20°$. The region from 71° to 90° in the (110) plane was not fitted using this technique since the contributing electrons are located in two small angular ranges and an adequate assignment of location could be made by a much simpler adjustment to the model positions. The polynomials derived in our fitting procedure are adequate to reproduce our final velocity distribution over the ranges to which they are applicable, although it should be realized that they are empirical tools and that no physical significance should be attached to their structure. The polynomial coefficients are found in Table I.

Several things determine the uncertainty in these velocity values. The equation used to determine the velocities is

$$v_{F_\perp} = \frac{\hbar}{e}(\omega)\left[\frac{h_p}{H_p}\right]^{2/3}(2K)_\perp^{1/3}$$

and it is evident from this that $\Delta v_F$ is dependent on $\Delta\omega$, $\Delta h_p$, $\Delta H_p$, and $\Delta K$ with these combined appropriately in quadrature, giving

$$\frac{\Delta v_F}{v_F} = \left\{\left[\frac{\Delta\omega}{\omega}\right]^2 + \frac{4}{9}\left[\left[\frac{\Delta h_p}{h_p}\right]^2 + \left[\frac{\Delta H_p}{H_p}\right]^2\right] + \frac{1}{9}\left[\frac{\Delta K}{K}\right]\right\}^{1/2}.$$

We estimate the field calibration used to be accurate to about $\pm 0.1\%$ while the reproducibility of a given peak was $\pm 0.4\%$, giving an overall uncertainty of $\pm 0.5\%$ for $H_p$. The microwave frequency $\omega$ is known to an accuracy of $\pm 0.13\%$. Although significant uncertainty ($\sim 10\%$) is attached to the parameter $\beta$ and $\sim 1\%$ to $\Gamma^*$, their effect on $v_F$ is about $\pm 1\%$ in the choice of $h_p$ for a given series. The estimate of $\Delta K$ is somewhat more difficult since it, in turn, depends on the uncertainties in several geometric values as well as the uncertainty in the FS model used in calculating $K$. The geometric uncertainties are $\sim 1°$ in sample-plane alignment, $\sim 1°$ in the determination of $\phi$, and $\sim 0.5°$ in the determination of $\theta$ and the assumption of a locally circular orbit. Of these, the latter has a small effect since the width of the band about the effective plane is on the order of 1°. To estimate its effect, we calculated $K$ at representative FS points over a range of 0.1° to 1° about the effective plane. Over this range, the variation in $K$ proved to be less than 0.1% for all points. The small ($\sim 0.2\%$) uncertainties in FS radii calculated from the Halse and Coleridge Ag7 fits may result in an additional uncertainty of several percent in the local radius of curvature, $K$. An estimate of this uncertainty can be made by finding values of $K$ using Fermi radii calculated from FS models using different numbers of terms in the SFE. We have performed such a calculation using the Halse Ag7 and Ag5 and the Coleridge Ag7 and Ag5 models. The difference in the $K$ value found from the Ag7 fit and from the corresponding Ag5 fit is typically

TABLE I. Coefficients of polynomials used in the iterative determination of the Fermi-surface locations of the contributing electrons.

| $C_0$ | $C_1$ | $C_2$ | $C_3$ | $C_4$ | $C_5$ |
|---|---|---|---|---|---|
| | | (100) ($\phi = 0°$ to $\phi = 20°$) | | | |
| 1.3465 | 0.032 781 | 5.8248 | −15.077 | 10.087 | 0 |
| | | (110) ($\phi = 0°$ to neck edge at 47.72°) | | | |
| 1.3478 | −0.041 439 | 9.8586 | −36.777 | 54.474 | −31.386 |
| | | (110) (neck edge at 61.76° to 71°) | | | |
| −1126.4 | 3979.9 | −5617.2 | 3962.8 | −1397.1 | 196.89 |

less than 4.5%. The uncertainty in $K$, based on these considerations, varies over the surface with the dependence of $K$ on location, reaching a maximum near the neck and having a mean value on the order of 5%. An exception to this is the value of $K$ used in analysis of the neck resonance. This was derived from curvature factors calculated for various models[15] and varies by less than 2% between models, leading to a somewhat higher precision in the calculation value of $v_F$ at the neck. The combination of these values yields an overall uncertainty in $v_F$ of $\pm 1.8\%$. Exceptions to this are the uncertainties at the $\langle 110 \rangle$ point in the (110) plane, where the low-amplitude signals observed lead to a greater uncertainty in $h_p$ and $H_p$ and an overall uncertainty of $\pm 2.2\%$, and the neck where the uncertainty is less than 1%.

The internal consistency of our results can be checked at the $\langle 100 \rangle$ point in the (100) and (110) planes, where a value of $v_F = 0.970$ was recorded in the (100) plane while a value of $v_F = 0.965$ was found in (110). This represents a difference of 0.6%, well within our calculated uncertainty.

## COMPARISON TO PREVIOUS RESULTS

Our final velocity distribution over the (100) and (110) zones is plotted in Fig. 5 along with those of Lengeler and Halse. Velocities at related values of $\phi$ are given, for all distributions, in Table II. It is immediately apparent in comparing these that the SLLR distribution reproduces the overall structure of the other two and in some ways represents a middle ground between them. Halse's velocities are quoted as being good to $\pm 3\%$ while Lengeler's are quoted as good to $\pm 1\%$, although at several points the two fits differ by more than their combined uncertainty, the largest differences being at $\langle 100 \rangle$ and at the neck where they differ by nearly 5%. By comparison, our velocity distribution differs from that of Lengeler by 4% at $\langle 100 \rangle$, and when the Halse Ag7 (Ref. 15) value for the curvature factor is used to calculate $K$, exact agreement is obtained at the neck. The largest difference from that of Halse is 3% at $\phi = 25°$ in the (110) plane. Over most of its range our distribution falls between the other two. Interestingly, the points at which it differs most widely

TABLE II. Fermi velocity values from present experiment and from dHvA experiments in free electron units (f.e.u.). The angle $\phi$ is the location on the Fermi surface measured from the $\langle 100 \rangle$ axis.

| | $v_F$ (f.e.u.: $v_0 = 1.39708 \times 10^8$ cm/s) | | |
|---|---|---|---|
| $\phi$ (deg) | Present work ($\pm 1.8\%$) | Halse ($\pm 3\%$) | Lengeler ($\pm 1\%$) |
| | (100) zone | | |
| $\langle 100 \rangle$ | 0.965 | 0.97 | 0.927 |
| 5 | 0.982 | 1.01 | 0.976 |
| 10 | 1.051 | 1.07 | 1.067 |
| 15 | 1.101 | 1.11 | 1.129 |
| 20 | 1.133 | 1.11 | 1.145 |
| 25 | | 1.10 | 1.132 |
| 30 | | 1.09 | 1.106 |
| 35 | | 1.07 | 1.081 |
| 40 | | 1.06 | 1.063 |
| $\langle 110 \rangle$ | 1.064 ($\pm 2.2\%$) | 1.05 | 1.056 |
| | (110) zone | | |
| $\langle 100 \rangle$ | 0.965 | 0.97 | 0.927 |
| 5 | 0.996 | 1.01 | 0.976 |
| 10 | 1.071 | 1.07 | 1.069 |
| 15 | 1.128 | 1.11 | 1.138 |
| 20 | 1.136 | 1.13 | 1.168 |
| 25 | 1.158 | 1.12 | 1.167 |
| 30 | 1.131 | 1.09 | 1.141 |
| 35 | 1.089 | 1.04 | 1.084 |
| 40 | 0.963[a] | 0.92 | 0.962 |
| 45 | 0.664[a] | 0.65 | 0.683 |
| neck | 0.371 ($\pm 1\%$) | 0.35[b] | 0.371 |
| 65 | 0.751[a] | 0.69 | 0.725 |
| 70 | 0.983 | 0.93 | 0.962 |
| 75 | | 1.02 | 1.043 |
| 80 | | 1.05 | 1.061 |
| 85 | | 1.05 | 1.059 |
| $\langle 110 \rangle$ | 1.064 ($\pm 2.2\%$) | 1.05 | 1.056 |

[a]Derived from polynomial fit.

[b]The value 0.35 is given in Table 10 of Ref. 2 based on the early dHvA data of Joseph and Thorsen (Ref. 16). A value of 0.37 is obtained from the cyclotron resonance mass of Henningsen (Ref. 17) quoted in Ref. 2.

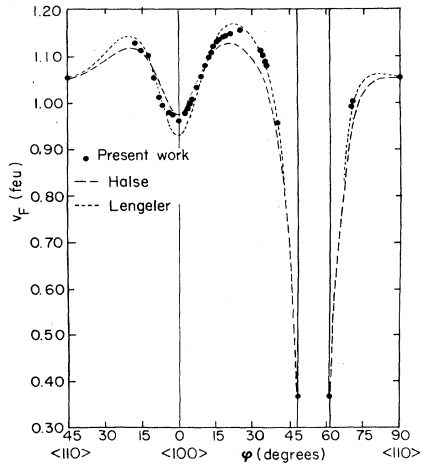


FIG. 5. Fermi velocity distributions over the (100) and (110) zones of Ag in units of free-electron velocity $v_0 = 1.397\,08 \times 10^8$ cm/sec.

from one or the other of the SFE distributions correspond to resonant series where we feel that the accuracy of our line-shape analysis and thus of our calculated $v_F$ is particularly good.

These differences are not, perhaps, unexpected since our determination of $v_F$ and those of Halse and Lengeler both depend in quite different ways on a detailed knowledge of the FS geometry. We make a local measurement of $v_F$, but one that is dependent on various approximations inherent in the theory, particularly with respect to $k_H$ broadening and its effects. As an example of the effect that $k_H$ broadening might have, we have calculated the angular range about ⟨100⟩ over which an average of Lengeler's $v_F$ values falls within our uncertainty range. Using a uniformly weighted average, this range is less than 6°, which corresponds closely to our estimate of the angular extent of the electron locations contributing to the SLLR signal. It should be noted that the Halse velocity distribution is derived from effective masses measured primarily from cyclotron resonance.[18] The measured values of the masses from cyclotron resonance should exhibit $k_H$ broadening effects and probably lead to a less anisotropic distribution than one derived from de Haas–van Alphen (dHvA) measurements. We also assume that the analytical expressions for the FS can be used to calculate highly local values of the radius of curvature, $K$, and the direction of the normal to the FS perimeter. The cyclotron mass inversions, on the other hand, are not really local measurements in any sense but they depend on deconvolutions of the measurements to produce local values. Bearing these distinctions in mind, we consider the correspondence between our distribution and those of Halse and Lengeler to be reasonable.

There is also reasonable agreement between our values of $v_F$ in the (100) plane and those derived from TFE measurements by Gantmakher *et al.*[6] The only significant differences between the two measurements are to the three TFE points taken from a (110) sample between 5° and 10° and given in Fig. 10 of Ref. 6. The agreement of the SLLR results with the TFE values taken from a (100) sample is excellent at all angles and the TFE values from the (110) sample agree well at angles greater than 10°.

## SUMMARY

In the present work we have generated measurements of the local values of the Fermi velocity of Ag over a wide region of the (100) and (110) central zones as well as at the neck in the (111) plane. The overall success of the experiment as compared to previous work[9,10] on Ag rests on our sample-preparation technique and our results confirm the utility of SLLR as a means of measuring Fermi-surface properties in metals.

There is an important difference in the velocity distributions derived from SLLR measurements and those obtained from dHvA cyclotron mass inversions. This difference is due to the fact that velocities derived from the SLLR, cyclotron resonance, and TFE measurements are averages over small angular ranges. In dHvA effective-mass measurements these averaging effects are much smaller and velocity distributions derived from them are closer to the actual distribution. These differences are apparent only at the turning points of highly anisotropic distributions, where the angular averages are quite different from the point values. The Lengeler distribution appears to be the best current estimate of the actual $v_F$ distribution for Ag, and care must be taken to use an appropriate angular average of these values when analyzing other measurements where angular broadening may be important.

## ACKNOWLEDGMENTS

We would like to thank Professor R. E. Doezema for several valuable discussions and for supplying us with a copy of the library of NKP characteristic spectra. This work was supported in part by the National Science Foundation under grant No. DMR-82-06116.

[1]P. T. Coleridge and I. M. Templeton, J. Phys. F **2**, 643, (1972); Phys. Rev. B **25**, 7818 (1982).
[2]M. H. Halse, Philos. Trans. R. Soc. London, Sect. A **265**, 507 (1969).
[3]B. Lengeler, W. R. Wampler, R. R. Bourassa, K. Mika, K. Wingerath, and W. Uelhoff, Phys. Rev. B **15**, 5493 (1977).
[4]R. E. Prange and Tsu-Wei Nee, Phys. Rev. **168**, 779 (1968); T. W. Nee, J. F. Koch, and R. E. Prange, *ibid.* **174**, 758 (1968); J. F. Koch and J. D. Jensen, *ibid.* **184**, 643 (1969).
[5]D. S. Falk, J. O. Henningsen, H. L. Skriver, and N. E. Christensen, Phys. Rev. B **6**, 377 (1972).
[6]V. F. Gantmakher, J. Lebech, and C. K. Bak, Phys. Rev. B **20**, 5111 (1979).
[7]R. E. Doezema and J. F. Koch, Phys. Rev. B **5**, 3866 (1972).
[8]M. J. G. Lee, Phys. Rev. B **2**, 250 (1970).
[9]J. O. Henningsen, Phys. Lett. **27A**, 693 (1968); **28A**, 392 (1968).
[10]P. Deimel and R. E. Doezema, Phys. Rev. B **10**, 4897 (1974).
[11]W. O. Hamilton and G. E. Pake, J. Chem. Phys. **39**, 2694 (1963). The material is 1,3-bisdiphenylene-2-phenylallyl (BDPA). It has a linewidth of ~0.75 Oe at 4.2 K and a $g$

factor of 2.002. We thank Professor Hamilton for kindly loaning us the sample.

[12]R. E. Doezema and J. F. Koch, Phys. Rev. B **6**, 2071 (1972).
[13]J. W. Mitchell and R. G. Goodrich, following paper [Phys. Rev. B **32**, 4977 (1985)].
[14]John W. Mitchell, Ph.D. dissertation, Louisiana State University, 1985.
[15]W. M. Bibby, P. T. Coleridge, N. S. Cooper, C. M. M. Nex, and D. Shoenberg, J. Low Temp. Phys. **34**, 681 (1979).
[16]A. S. Joseph and A. C. Thorsen, Phys. Rev. **138**, A1159 (1965).
[17]J. O. Henningsen, Phys. Status Solidi **32**, 239 (1969).
[18]D. G. Howard, Phys. Rev. **140**, A1705 (1965).